

Correlation between grain boundary energy and geometry in Ni-rich NiAl

Yaron Amouyal^{a,*}, Eugen Rabkin^a, Yuri Mishin^b

^a Department of Materials Engineering, Technion–Israel Institute of Technology, Technion City, 32000 Haifa, Israel

^b School of Computational Sciences, George Mason University, Fairfax, VA 22030, USA

Received 30 January 2005; received in revised form 7 April 2005; accepted 12 April 2005

Available online 17 June 2005

Abstract

The relative energies of 43 different large angle grain boundaries in Ni-rich NiAl have been determined with the aid of scanning probe microscopy using the thermal grooving method at 1400 °C. Simultaneously, the geometrical degrees of freedom of the same grain boundaries have been characterized by a combination of electron back-scattering diffraction and serial sectioning techniques. The determined values of the ratio of the grain boundary to surface energy are scattered over a wide range of 0.2–1.1. It is found that twist grain boundaries exhibit higher energies than their tilt counterparts. Moreover, mixed grain boundaries with approximately equal amount of tilt and twist components do not exhibit high energies. A strong dependence of the energy of a large angle grain boundary with fixed misorientational degrees of freedom on its plane inclination has been demonstrated. The energies of several selected grain boundaries and free surfaces in NiAl have been calculated by employing an embedded-atom method (EAM) interatomic potential specially developed for NiAl. The range of possible relative grain boundary energies estimated from these calculations is in a good agreement with experimental data.

© 2005 Acta Materialia Inc. Published by Elsevier Ltd. All rights reserved.

Keywords: Grain boundary energy; Grain boundary structure; Electron back-scattering diffraction; Atomic force microscopy

1. Introduction

The NiAl intermetallic compound exhibits many attractive engineering properties such as high melting temperature, high oxidation resistance, high modulus of elasticity, low density, and metal-like thermal and electrical conductivity [1–4]. However, the main obstacles which still prevent NiAl from being widely applied are its low-temperature brittleness and poor high-temperature creep resistance. For more than three decades, attempts to improve NiAl ductility by controlled alloying with other elements have been unsuccessful [4–7].

It was found that the brittleness of polycrystalline NiAl is always associated with intergranular brittle fracture along grain boundaries (GBs). The character of GBs in metals may substantially dictate their physical properties. Creep behaviour is related directly to GB diffusivity, while intergranular brittleness and corrosion behavior correlate with GB energy. Lowering the GB energy should result in a decrease of the intergranular brittleness [2,3,8,9]. Both GB energy and diffusivity depend sensitively on GB geometry, i.e., on the misorientation parameters of two neighboring grains forming a GB and on the inclination of the GB plane. This dependence is a cornerstone of the new concept of grain boundary engineering (GBE). The essence of GBE is an increase, by a suitable thermomechanical treatment, of the population of GBs with geometry minimizing or maximizing certain physical parameter [10–16]. For

* Corresponding author. Tel.: +972 4 829 3875; fax: +972 4 829 5677.

E-mail addresses: amouyal@tx.technion.ac.il (Y. Amouyal), erabkin@tx.technion.ac.il (E. Rabkin), ymishin@gmu.edu (Y. Mishin).

instance, in metals with low stacking fault energy an increase in the fraction of coherent twin boundaries in the GB populations considerably diminishes the probability of intergranular brittle fracture [17]. For successful application of the GBE concept, knowledge of the relationship between GB properties and GB geometry is required.

For a macroscopic geometrical description of a GB three misorientational degrees of freedom (DOFs) of the two adjacent grains are firstly required. Additional DOFs are associated with orientation of the GB plane in the frame of reference of one of the two grains, which gives two additional independent parameters. These five parameters together give a full macroscopic description of GB geometry in terms of macroscopic, geometrical DOFs [10,18–24]. The dependence of GB energy on all five geometrical DOFs is still the subject of controversy [10,25–31]. For diluted face-centered cubic (fcc) metallic alloys Wynblatt and Takashima [32] suggested a model based on the matching of two terraced surfaces forming a GB that provided a good description of experimental data. Rohrer and co-workers [33] have demonstrated that in ceramics there is a reasonable correlation between the sum of energies of two surfaces forming a GB and the energy of this GB. To our knowledge, no attempts have been undertaken so far to correlate the energy of GBs with their macroscopic geometrical DOFs in ordered intermetallic compounds. Knowledge of such a correlation is necessary for evaluating the potential of GBE in improving properties of polycrystalline NiAl. In this work, we employed a thermal grooving technique for measuring the relative energies of GBs in Ni-rich NiAl. Special care has been exercised to avoid possible effects of near-GB lattice rotations [9] and of surface anisotropy [34] on measured GB energies.

2. Experimental methods

Ingots of polycrystalline Ni-rich NiAl with an average grain size of about 500 μm were produced by repeated re-melting under vacuum in a silver crucible cooled with pressurized water. Three to four remeltings were performed in order to obtain a sufficient homogeneity of chemical composition and coarse grains. Samples of about 1–2 cm in diameter and 4 mm in thickness were cut from the ingot and polished by SiC papers and diamond pastes down to 0.25 μm particle size. Their chemical composition was determined with the aid of a Philips XL30 scanning electron microscope (SEM) equipped with a LINK ISIS (Oxford Instruments, UK) energy dispersive X-ray spectrometer (EDS). The accelerating voltage was 20 keV with the 1 nA probe current. X-ray radiation with the 30° take-off angle was used, from which the Ni $K\alpha$ and Al $K\alpha$ analytical lines were analyzed and calibrated with pure

Ni and Al standards. The acquisition time was 100 s. The final results were averaged over seven measurements per sample and normalized to 100%. The chemical composition of these Ni-rich NiAl specimens was established to be 45.6 ± 0.2 at.% Al.

All thermal grooving annealings were conducted in a ultra-high vacuum (UHV) home-designed furnace described elsewhere [35]. The samples were annealed for 30 min at 1400 °C in the vacuum of 10^{-7} Torr. No surface oxidation was observed under these conditions. As a result of the annealing process, a reduction in the Al content in the near-surface region was observed. The chemical composition of the Ni-rich specimens after annealing was 41.0 ± 0.3 at.% Al. The EDS analyses indicated that this Al depletion extends to the depth of about 100 μm beneath the surface. Scanning probe microscopy (SPM) measurements were performed with the AutoProbe CP SPM (Park Scientific, USA) operated in the contact mode. W₂C-coated CSC11/50 Ultrasharp Si tips manufactured by NT-MDT (Russia) with the nominal radius of curvature of 50 nm were used. The SPM images contained 256 × 256 pixels and were taken in the region of the GB grooves, with the scanning direction being approximately perpendicular to the groove. The raw data were analyzed with the SPM-integrated PSI ProScan image processing software in order to correct for instrumental distortions.

Crystallographic orientations of individual grains were determined by the electron back-scattering diffraction (EBSD) method. The acquisition of EBSD patterns (EBSPs) was performed with the LINK OPAL System (Oxford Instruments, UK) mounted on the high-resolution field emission gun SEM (HRSEM) LEO982 Gemini (Zeiss-Leica). The EBSPs were taken under the following conditions: accelerating voltage 20 keV, beam current ~ 3 nA, working distance 21 mm with the sample holder tilted by 70° to the primary beam. Diffraction patterns have been taken in the magnification range of 10,000–30,000 from regions that were not too close to the GB groove, in order to avoid EBSP noise. The EBSPs were recorded on a CCD and automatically analyzed by the LINK OPAL software. Each EBSP yielded a rotation matrix [R] with an angular accuracy of about 2°. This matrix is determined with respect to a fixed reference system (the axes of the HRSEM specimen holder). The misorientation matrix of each GB could be calculated using [R] matrixes of the two adjacent grains, which yields three misorientational DOFs of this GB. The combined SPM and EBSD measurements for an individual GB are demonstrated in Fig. 1.

SEM images were acquired with the aid of HRSEM described above with the annular in-lens detector, accelerating voltage of 20 keV and working distance of 5 mm. Optical microscopy measurements were conducted with a Zeiss microscope.

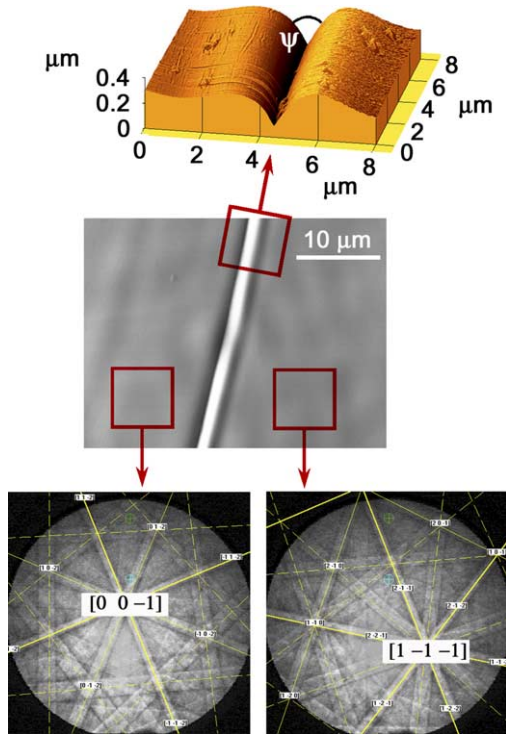


Fig. 1. Schematic illustration of a thermal groove characterization by SPM and of determining the misorientational DOFs of a GB by EBSD.

Micro-indentations for the assessment of the GB plane inclination were performed with a Vickers Microhardness indenter (Buhler) using the load of 1 kgf for 10 s. The Vickers diamond indenter has a pyramidal shape with an apex angle of 136°.

2.1. SPM characterization of GB grooves

In each sample, only GB grooves satisfying the following conditions were selected for analysis:

- (i) The groove profile at the root should be sharp, rather than rounded.
- (ii) The groove profile should be nearly symmetric.
- (iii) The surface in the vicinity of the groove should not be faceted.

These selection rules ensure that the GB is indeed located beneath the groove root and that the surface energy is nearly isotropic [9,34]. The relative GB energy (the ratio of GB energy and surface energy), γ_{rel} , is then given by the following relationship:

$$\gamma_{\text{rel}} = 2 \cdot \cos\left(\frac{\psi}{2}\right), \quad (1)$$

where ψ is the dihedral angle at the root of the GB groove. The selection criteria (ii) and (iii) ensure that the effect of surface torque terms on the measured values of γ_{rel} is minimal and, therefore, they were neglected in

Eq. (1). The values of ψ and γ_{rel} were calculated by averaging the data for each of the 256 SPM topography line profiles running perpendicular to the trace of GB groove. The value of ψ for each individual line profile was obtained by parabolic interpolation of the topography data points in the vicinity of the groove root (see [36] for details).

2.2. Tip radii measurements

It has been reported earlier that the angle ψ measured by SPM suffers from a systematic error due to the finite tip curvature [37–39]. Assuming that the rounding of the SPM tip is a sphere of radius R , the corresponding correction to ψ can be easily calculated:

$$\Delta\theta = \frac{2aR \cdot \sin\theta}{1 + \tan^2\theta}, \quad (2)$$

where $\theta \equiv 90^\circ - \psi/2$ and a is the parabolic coefficient in the Taylor expansion of the groove profile. The radius R can be measured with the aid of HRSEM. However, the tip wear rate during the scanning of the relatively hard NiAl is high and R changes from image to image. Measuring R after the imaging of each individual GB groove would not be practical. Therefore, we have developed a special method for taking into account the time-dependent wear of SPM tips. The whole population of GBs is divided into several groups containing each about 10 GBs. For each group, the tip curvature is measured by HRSEM before and after a series of measurements. Assuming that R increases linearly with the increasing “mileage” that a given tip has traveled along the surface of the sample, the tip radius of curvature for the n th measurement, R_n , can be obtained by linear interpolation. Thus, the correction for the relative energy of the n th GB in the group can be obtained by:

$$\Delta\gamma_{\text{rel}} = 2aR_n \frac{\sin(2\theta)}{1 + \tan^2\theta}. \quad (3)$$

2.3. GB plane inclination measurements

Two inclinational DOFs of all GBs were determined by measuring the angles of the GB groove line (on the SEM image) with respect to the specimen holder axes and using serial sectioning. As illustrated in Fig. 2, the unit GB plane normal vector \vec{N} is expressed as:

$$\vec{N} = (\cos\alpha \cdot \cos\beta, \cos\alpha \cdot \sin\beta, \sin\alpha), \quad (4)$$

where α and β are the inclination angles of \vec{N} with respect to the Z - and X -axes. The $\{XYZ\}$ coordinate system is defined with reference of the specimen holder stage in the HRSEM. The Z -axis is normal to the stage, while X - and Y -axes correspond to the rolling and transverse directions, respectively. The latter two axes are clearly marked on the specimen holder stage.

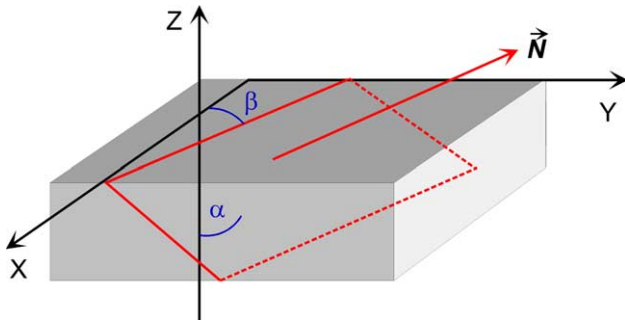


Fig. 2. Definition of the GB plane normal in terms of the in-plane inclination β and the “hidden” inclination α , defined with respect to a fixed Cartesian coordinate system.

In the process of serial sectioning [18,40,41], two micro-hardness indents are made on both sides of each GB groove imaged previously in the SPM. Their lateral size, X_i , and the distance from the groove line, Y_i , are measured by optical microscope. After a slight polishing and etching with Kroll’s reagent ($\text{H}_2\text{O} + 4\% \text{vol. HNO}_3 + 2\% \text{vol. HF}$) [42] the apparent sizes of the indents diminished and their distances from groove changed (Fig. 3). The depth of polishing is calculated from the change in the sizes of the indents under the assumption that the dihedral angle at the root of a Vickers indent coincides with the apex angle of the diamond indenter and is equal to 136° . The “hidden” inclination of the GB plane with respect to the sample surface, α , is calculated according to:

$$\alpha = \tan^{-1} \left(2\sqrt{2} \cdot \tan(136^\circ/2) \frac{Y_f - Y_i}{X_f - X_i} \right), \quad (5)$$

where X_f and Y_f are the lateral sizes of the indents and their distances from the groove line, respectively, after the polishing.

To summarize the experimental procedure, we employ SPM to measure the dihedral angles at the root of several carefully pre-selected GB grooves. The selection procedure is aimed to minimize the effects associated with surface anisotropy. The relative GB energy, γ_{rel} , is determined using Eq. (1). For the same set of

GBs, three misorientational DOFs $[UVW]$, θ are obtained with the aid of EBSD analysis in SEM. The two inclinational DOFs, \vec{N} , are determined using serial sectioning and measuring the orientation of GB groove lines with respect to the SEM reference frame. The dependence $\gamma_{\text{rel}}(\{\text{DOFs}\})$ for all GBs studied here constitutes the main experimental result of the present work.

3. Results

3.1. Relative GB energy

The values of the relative energy for all 43 GBs studied in this work are given in Table 1. The energies are corrected for the finite tip radius [see Eq. (3)]. The error bar of the GB energy is the statistical standard deviation of individual γ_{rel} values calculated for each of the 256 line profiles taken from a particular SPM image. It follows from Eq. (3) that the systematic error $\Delta\gamma_{\text{rel}}$ associated with the finite tip radius is more significant for larger values of the GB energy, which correspond to small dihedral angles. In this study, the values of $\Delta\gamma_{\text{rel}}$ were slightly higher than the statistical errors of γ_{rel} only for few high-energy GBs. Therefore, it can be concluded that the correction for the finite tip radius was of marginal importance in this study, mainly because of the frequent tip replacements, the use of coated tips with decreased wear rates (all tip radii were below 120 nm) and the relatively large lateral dimensions of the grooves.

3.2. GB geometry

The EBSD analyses performed on both sides of the GBs characterized by SPM yielded a list of rotation matrices pairs, $[R_1]$ and $[R_2]$, for each GB. From all 24 equivalent misorientation axis/angle pairs the disorientation representation was selected [18,23]. Thus, the three misorientational DOFs of every GB ($[U, V, W]$, θ) were determined. These data, together with the two

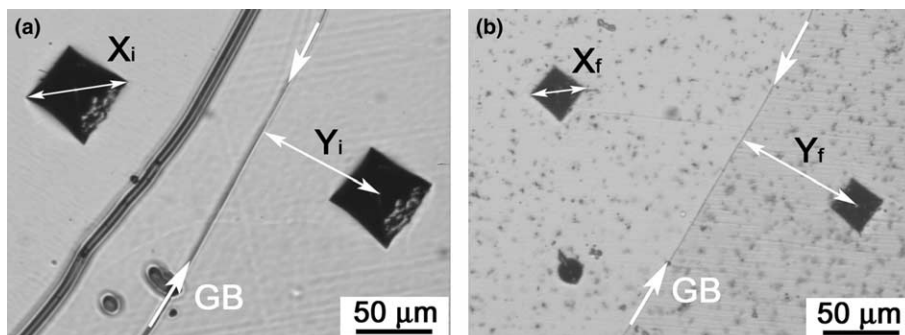


Fig. 3. Two optical microscope images of the same GB marked with Vickers microhardness indents (a) before and (b) after polishing and etching.

Table 1
The list of all investigated GBs

GB no.	Disorientation Axis/angle (°)	GB planes	φ (°)	CSL misorientation Axis/angle (°)	Angular deviation (°)	γ_{rel}
1	[0.86, 0.44, 0.25] 40.0	(0.72, 0.36, -0.59) (-0.82, 0.17, 0.55)	148			0.63 ± 0.02
2	[0.90, 0.33, 0.29] 49.0	(0.21, -0.86, -0.46) (0.30, -0.15, -0.94)	72	[3, 1, 1], 50.7° $\Sigma = 15$	1.63	0.59 ± 0.02
3	[0.76, 0.63, 0.13] 49.6	(-0.20, -0.48, -0.86) (-0.65, 0.50, -0.57)	8			0.45 ± 0.02
4	[0.80, 0.47, 0.38] 45.0	(-0.33, -0.81, 0.48) (-0.99, 0.03, -0.17)	5	[2, 1, 1], 44.4° $\Sigma = 21\text{b}$	2.36	0.45 ± 0.01
5	[0.96, 0.27, 0.05] 15.6	(0.76, 0.47, 0.45) (0.25, 0.89, -0.39)	176			0.48 ± 0.05
6a		(0.52, -0.33, 0.79) (0.66, 0.21, -0.72)	140			0.67 ± 0.03
6b		(0.61, -0.45, 0.66) (0.63, 0.40, -0.67)	140			0.94 ± 0.02
6c		(0.71, -0.43, 0.56) (0.68, 0.48, -0.56)	135			0.47 ± 0.04
6d	[0.66, 0.62, 0.43] 48.9	(0.82, -0.42, 0.38) (0.69, 0.61, -0.4)	138			0.97 ± 0.01
6e		(0.88, -0.39, 0.28) (0.70, 0.66, -0.28)	140			0.74 ± 0.03
6f		(0.97, -0.25, 0.02) (0.70, 0.72, 0.02)	143			1.01 ± 0.01
6g		(-0.55, 0.83, 0.09) (-0.10, -0.94, 0.32)	146			0.60 ± 0.03
6h		(-0.48, 0.87, 0.15) (0.00, -0.95, 0.30)	146			0.74 ± 0.01
7	[0.85, 0.50, 0.13] 36.4	(0.06, -0.87, 0.49) (-0.34, -0.67, 0.67)	24			0.81 ± 0.02
8	[0.91, 0.33, 0.27] 30.6	(0.02, 0.60, 0.80) (-0.70, -0.70, 0.19)	147			0.58 ± 0.04
9	[0.91, 0.41, 0.12] 30.6	(-0.52, -0.09, -0.85) (0.57, 0.41, -0.71)	145			0.96 ± 0.01
10	[0.94, 0.34, 0.07] 39.6	(0.95, 0.31, -0.03) (-0.61, 0.77, -0.20)	125			0.52 ± 0.01
11	[0.69, 0.62, 0.37] 24.7	(-0.39, -0.79, -0.48) (-0.76, 0.65, 0.00)	82			0.37 ± 0.01
12	[0.68, 0.61, 0.41] 54.5	(-0.90, -0.20, -0.39) (-0.39, 0.74, -0.55)	15			0.32 ± 0.02
13	[0.64, 0.59, 0.49] 51.4	(-0.33, 0.60, 0.73) (0.42, -0.37, 0.83)	11			0.37 ± 0.02
14	[0.81, 0.51, 0.29] 32.4	(-0.43, 0.22, -0.88) (1.00, 0.02, 0.00)	111			0.57 ± 0.04
15	[0.82, 0.52, 0.25] 25.2	(0.92, 0.36, -0.15) (0.98, 0.14, 0.17)	11			0.21 ± 0.01
16	[0.62, 0.57, 0.53] 60.0	(-0.56, 0.45, -0.70) (0.48, 0.54, 0.70)	144	[1, 1, 1], 60° $\Sigma = 3$	3.5	0.39 ± 0.02
17	[0.70, 0.62, 0.36] 45.7	(0.41, 0.81, 0.42) (0.25, -0.84, -0.48)	163	[2, 2, 1], 46.4° $\Sigma = 29\text{a}$	2.46	0.86 ± 0.01
18	[0.85, 0.41, 0.32] 42.9	(0.91, 0.16, -0.38) (0.60, -0.48, 0.64)	23			0.43 ± 0.02
19	[0.91, 0.38, 0.18] 32.6	(-0.02, -0.64, 0.77) (0.17, -0.42, 0.89)	27			0.49 ± 0.01
20	[0.90, 0.41, 0.18] 49.2	(-0.56, -0.47, -0.68) (0.84, 0.14, 0.52)	154			0.71 ± 0.02
21	[0.76, 0.64, 0.14] 35.7	(0.53, -0.05, -0.84) (0.79, 0.35, -0.50)	120			0.95 ± 0.01
22	[0.93, 0.27, 0.26] 45.7	(-0.42, -0.66, -0.63) (-0.49, 0.18, 0.86)	130			0.91 ± 0.02
23	[0.64, 0.58, 0.50] 50.4	(-0.77, -0.05, 0.64) (-0.36, -0.21, 0.91)	41	[1, 1, 1], 60° $\Sigma = 3$	3.69	0.91 ± 0.02
24	[0.75, 0.66, 0.06] 40.0	(0.88, 0.00, -0.47) (-0.84, -0.24, 0.49)	178	[1, 1, 0], 38.9° $\Sigma = 9$	4.13	0.92 ± 0.01

(continued on next page)

Table 1 (continued)

GB no.	Disorientation Axis/angle (°)	GB planes	φ (°)	CSL misorientation Axis/angle (°)	Angular deviation (°)	γ_{rel}
25	[0.73, 0.68, 0.04] 58.5	(0.81, 0.40, 0.44) (−0.78, −0.35, 0.53)	147			0.70 ± 0.02
26	[0.83, 0.55, 0.10] 19.2	(0.16, −0.34, −0.93) (0.27, −0.80, 0.54)	78			0.41 ± 0.01
27	[0.96, 0.26, 0.04] 46.0	(0.96, −0.27, −0.02) (0.86, 0.48, −0.16)	13			1.06 ± 0.02
28	[0.75, 0.64, 0.16] 37	(0.95, −0.13, −0.28) (−0.31, 0.41, −0.86)	63			0.63 ± 0.02
29	[0.87, 0.45, 0.20] 21.9	(−0.72, −0.62, −0.30) (0.69, 0.05, −0.72)	168			0.92 ± 0.01
30	[0.75, 0.64, 0.17] 48.2	(0.22, −0.83, 0.51) (−0.20, 0.87, 0.46)	149			0.79 ± 0.01
31	[0.76, 0.65, 0.07] 37.4	(−0.06, −0.58, −0.81) (0.20, 0.97, 0.12)	160	[1, 1, 0], 38.9° $\Sigma = 9$	4.13	0.61 ± 0.01
32	[0.93, 0.32, 0.19] 41.7	(−0.42, 0.89, 0.16) (−0.47, 0.52, −0.71)	155			0.75 ± 0.01
33	[0.69, 0.54, 0.48] 37.1	(−0.52, −0.07, −0.85) (−0.97, −0.08, −0.23)	145			0.80 ± 0.02
34	[0.72, 0.69, 0.11] 36.2	(−0.35, −0.76, 0.55) (0.67, 0.63, −0.40)	164	[1, 1, 0], 38.9° $\Sigma = 9$	5.08	0.26 ± 0.03
35	[0.83, 0.55, 0.02] 37.5	(0.08, −0.33, 0.94) (0.94, −0.35, 0.08)	1			0.84 ± 0.01
36	[0.73, 0.67, 0.12] 22.8	(0.19, 0.97, −0.13) (0.08, −0.87, −0.49)	170			0.57 ± 0.01

The macroscopic geometrical DOFs of the GBs are given both in the disorientation scheme (second column) and the interface-plane scheme (third and fourth columns). The closest CSL disorientations (if any, according to the Brandon criterion) and the corresponding angular deviations are given in the fifth and sixth columns, respectively. The relative GB energies are given in the seventh column.

inclinational DOFs [denoted by \vec{N} , Eq. (4)], represent the full set of five DOFs for every GB. An alternative description of GB geometry is given by the interface-plane representation [18]. According to this scheme, the GB geometry is characterized by two GB plane normals corresponding to the grains and an angle of relative twist between the planes, $(\vec{n}_1, \vec{n}_2, \varphi)$. The angular accuracy of both representations is determined by the accuracy of EBSD measurements ($\pm 2^\circ$) and by the statistical error in measuring the angles α and β (see Fig. 2), which were 3° and 2° , respectively. The overall angular accuracy of the data presented in Table 1 is estimated to be about 4° .

3.3. Dependence of GB energy on inclinational DOFs

One of the GBs (GB no. 6) was significantly curved and therefore exhibited a variable inclination while the three misorientational DOFs were fixed (Fig. 4). This GB migrated from its original (OGB) toward final (FGB) position leaving behind numerous ghost lines. Both SPM scans and the measurements of the GB plane inclination were made in eight regions A–H marked by squares in Fig. 4. These sections of the individual GB were considered as different GBs, designated as 6a, 6b, ..., 6h, exhibiting identical misorientations. Fig. 5 shows the dependence of the relative GB energy on the apparent inclination angle β . Although the value

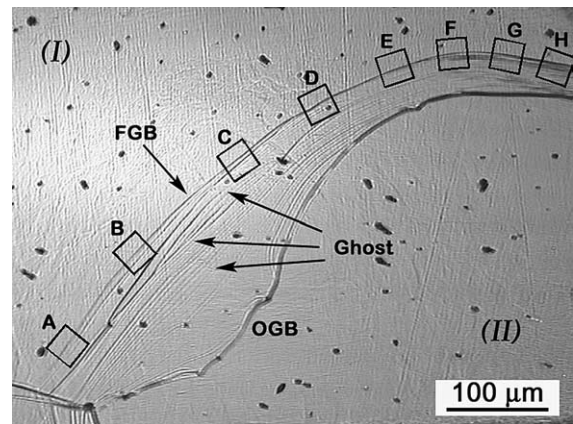


Fig. 4. Optical microscope image of GB no. 6. The squares designate the regions where SPM scans were performed and the angles α and β were measured.

of β is not related directly to the GB crystallography, this dependence demonstrates qualitatively the effect of GB plane inclination on the GB energy for a GB with the fixed misorientational DOFs [332], 49° .

3.4. Plane-matching GBs

In so-called plane-matching GBs, certain low-index lattice planes in two adjacent grains forming the GB are parallel to each other. It has been argued that

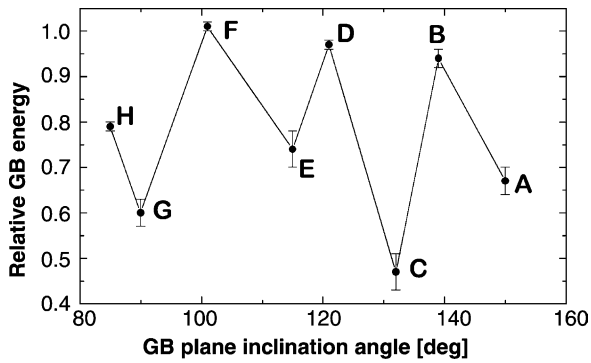


Fig. 5. Dependence of the relative energy of GB no. 6 on the in-plane inclination angle.

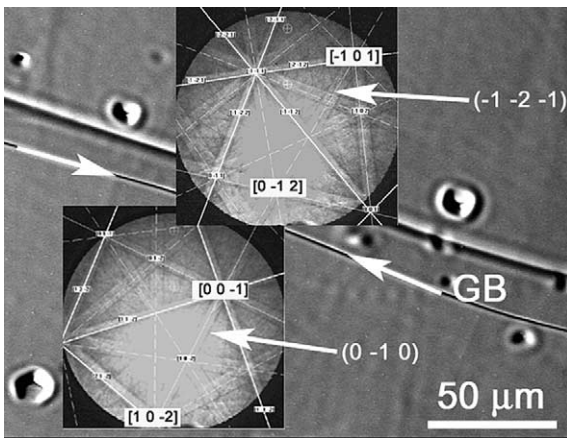


Fig. 6. HRSEM image of a GB with the relative energy of 0.86 ± 0.01 . The two EBSPs illustrate the matching of the $\{211\}\{100\}$ planes.

plane-matching GBs should be classified as “special boundaries” since they exhibit low energy, good corrosion resistance, etc. [43,44]. As a property that depends on the misorientation only, the plane-matching configuration can be readily identified from the comparative analysis of two EBSPs taken from the adjacent grains. Fig. 6 shows an example of plane matching across a GB. The pairs of EBSPs for all GBs with different misorientations have been analyzed to determine whether these GBs belong to the plane-matching type and whether the plane-matching GBs exhibit particularly low energies. It has been found that out of 36 GBs with different misorientational DOFs, 20 were of the plane-matching type. They comprised all possible combinations of the $\{211\}$, $\{110\}$ and $\{100\}$ planes and exhibited a wide spectrum of relative energies.

4. Discussion

4.1. Relative GB energy

The relative GB energies listed in Table 1 range between 0.21 and 1.06. While for large angle GBs in pure

metals it is generally accepted that $\gamma_{\text{rel}} \leq 0.5$ [45], the values of γ_{rel} as high as 1.5 are not uncommon in ceramics [39]. Therefore, on the scale of GB energies, the Ni-rich NiAl compound occupies a position intermediate between pure metals and ceramics. This is not surprising taking into account strong Ni d- and Al p-hybridization along $\langle 111 \rangle$ directions between nearest neighbor Ni and Al atoms in the NiAl lattice [46]. This directional, covalent-type atomic bonding constrains the relaxation of atomic positions in GBs, which can result in high-GB energies. Since for brittle intergranular fracture the energy of fracture decreases with increasing GB energy, the intergranular brittleness of NiAl can be its intrinsic property.

It should be noted that γ_{rel} values as high as 0.8 and 1.6 were observed in Bi-doped Cu bicrystals [47] and in Inconel 600 alloy [48], respectively. In both cases, the alloying elements can exhibit a stronger tendency to surface rather than GB segregation, which would result in the surface energy decreasing faster than GB energy with increasing the amount of the alloying additions. This can explain the observed increase in γ_{rel} . In addition, the alloying elements can significantly increase the interfacial anisotropy, which is well-documented for the Cu–Bi system [49]. In the latter case, GB grooves can be faceted on the microscale and the use of Eq. (1) can lead to erroneously high values of γ_{rel} . In fact, strong surface faceting in the vicinity of a GB groove root in the Cu-160ppm. Bi bicrystals has recently been demonstrated [50]. The careful selection of non-faceted grooves in the present study helped us to minimize the possible problems associated with surface anisotropy.

The experimentally measured relative GB energies correlate closely with results of atomistic computer simulations. The simulations were performed using the EAM potential for NiAl developed in [51] by fitting to a large database of experimental and first-principles data. This potential has recently been applied to study surface structure and segregation [52,53], point defects [51,54], diffusion [55] and other properties of NiAl. In the present work, a GB was created by joining two grains with chosen orientations along a desired GB plane. The boundary conditions were periodic in the directions parallel to the GB plane and fixed in the normal direction [56]. The ground state structure of the GB was obtained by minimizing the total energy of the simulation block with respect to local atomic displacements as well as relative rigid translations of the grains. The rigid translations are required for the structural relaxation of the boundary with respect to its microscopic DOFs. The stability of the GB structure found by this procedure was verified by a normal-mode analysis using the dynamical matrix of the system. The GB energy at $T=0$ K was determined by comparing the relaxed total energy of the block

with the energy of perfect NiAl lattice containing the same amount of Ni and Al atoms, and dividing this energy difference by the GB area. A similar methodology was applied to compute surface energies in NiAl. The surfaces were created by a cleavage of the perfect lattice along a desired crystal plane followed by full atomic relaxation.

The calculated energies of four symmetrical tilt GBs (STGBs) and six low-index surfaces in stoichiometric NiAl are shown in Tables 2 and 3, respectively. The GB plane in the $\Sigma 5$ [001] STGBs can be either Ni- or Al-rich, which affects the value of the GB energy. The Al-centered GBs are marked by an asterisk in Table 2. For the surfaces at which both Ni and Al terminations are possible, an average of the two is presented. The average energy for all surfaces simulated is $\bar{\gamma} = 1.53 \text{ J/m}^2$. The values of γ_{rel} presented in the last column of Table 2 have been calculated using this average surface energy. GB no. 16 (Table 1) is an experimentally found GB with geometrical DOFs closest to the simulated $\Sigma = 3$ GBs (deviation of 3.5° from the exact $\Sigma 3$ misorientation). Its experimentally measured energy is $\gamma_{\text{rel}} = 0.39 \pm 0.02$, which lies between the higher and lower calculated values for the $\Sigma 3$ GBs. Thus, the agreement between the theory and experiment is satisfactory in this respect.

From the data presented in Tables 2 and 3, a rough estimate of the possible range of relative GB energies can be made by dividing the minimal GB energy by the maximal surface energy, and vice versa: $0.28 < \gamma_{\text{rel}} < 0.92$. This estimate is also very close to the experimentally determined range of relative GB energies (0.21–1.06), which validates our experimental measurements. An example of a calculated GB atomic structure is pre-

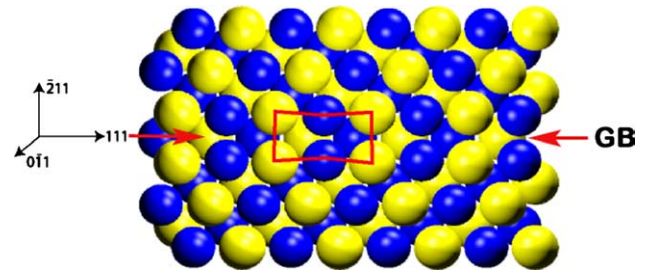


Fig. 7. Cross-section of the calculated atomic structure of the $\Sigma 3$ (211)[011] GB in stoichiometric NiAl.

sented in Fig. 7. It can be seen that individual atomic relaxations at the GB core are indeed relatively small.

It should be noted that our experimental measurements of the GB energies were performed on a Ni-41.0 \pm 0.3 at.% Al alloy, while a stoichiometric compound was modeled in our computer simulations. The GB energy depends on the bulk composition and, therefore, a direct comparison of the experimental data with the results of the simulations is not possible. However, such dependence is minor in comparison with the dependence of the GB energy on the geometrical DOFs. Indeed, in the calculations of Xie and Mishin [57] it was shown that the excess GB free energy changes by a maximum of 20% over the entire range of Ni bulk concentrations from the stoichiometry to the solubility limit. This is much smaller than both the experimentally measured and calculated variations in the GB energy associated with the geometrical DOFs. Therefore, the dependence of GB energy on Ni content cannot change the main conclusions of this work.

4.2. GB geometry

4.2.1. GB energy as a function of inclinational DOFs

The special case of GB no. 6 (Table 1) allows us to separate the dependence of the GB energy on the two inclinational DOFs from its dependence on the misorientational DOFs. The striking feature of Fig. 5 is the strong non-monotonic dependence of the GB energy on the inclination (γ_{rel} varies by a factor of two). This indicates that interfacial anisotropy in Ni-rich NiAl is high. It should be noted that none of the eight GBs A–H exhibited a low energy.

Fig. 5 shows the dependence of γ_{rel} on only one, in-plane inclinational DOF. A more informative presentation can be obtained in three dimensions by displaying γ_{rel} values in two (100)–(110)–(111) stereographic triangles, one for each grain (I and II in Fig. 4) joining along the GB (see Fig. 8). In this figure, the bars labeled by A–H (according to the notation mentioned above) designate the relative GB energies. This way the dependence of the GB energy on four macroscopic DOFs (out of five) is visualized. This presentation leads to the following observations:

Table 2

Absolute values of energies of STGBs energy in NiAl at $T = 0 \text{ K}$ calculated using an EAM interatomic potential

STGB	Energy (J/m^2)	γ_{rel}
$\Sigma 5$ (210)[001]	0.980	0.641
$\Sigma 5$ (210)[001]*	0.886	0.579
$\Sigma 5$ (310)[001]	1.066	0.697
$\Sigma 5$ (310)[001]*	1.148	0.750
$\Sigma 3$ (211)[011]	0.459	0.300
$\Sigma 3$ (111)[011]	0.734	0.480

Al-centered GBs are marked by an asterisk.

Table 3

Absolute values of surface energies in NiAl at $T = 0 \text{ K}$ calculated using an EAM potential

Surface	Energy (J/m^2)
(100)	1.640
(110)	1.251
(111)	1.633
(211)	1.503
(210)	1.547
(310)	1.613

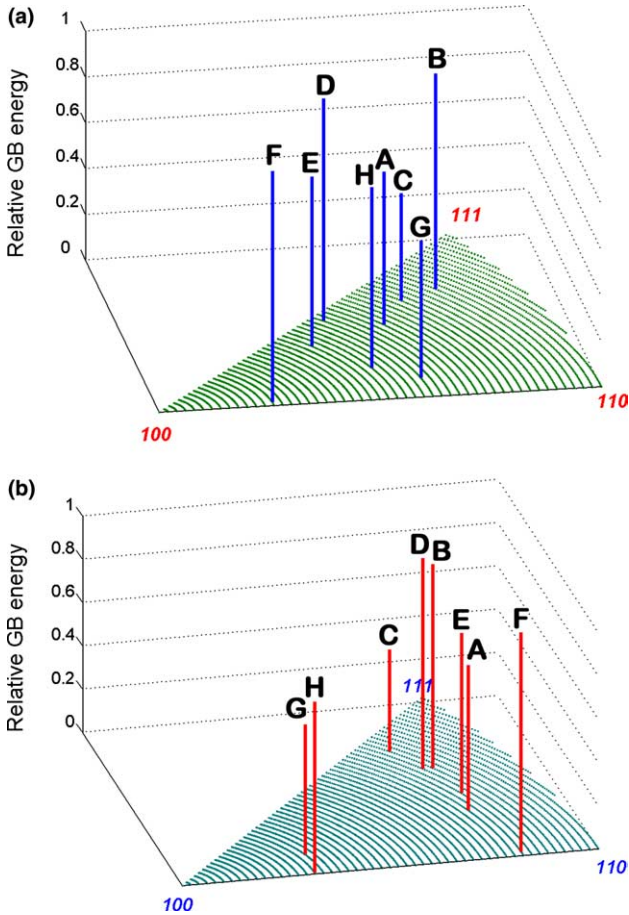


Fig. 8. Dependence of the relative GB energy on crystallographic parameters of the GB plane in two adjacent grains (I and II). The letters A–H refer to eight positions along GB no. 6 shown in Fig. 4.

- Each one of the GBs *B* and *C* is composed of two crystal planes laying close to each other in the $\{111\}$ region of the stereographic triangle. Therefore, these GBs are close to the class of pure twist GBs. In spite of that they exhibit very different energies.
- The GBs with at least one plane laying on the $\{100\}$ – $\{110\}$ axis of the stereographic triangle exhibit high energies.

An interesting feature of Fig. 4 is the presence of a flat GB facet at the position of the lowest energy (labeled by C). Assuming that the GB runs perpendicular to the surface, the condition of mechanical equilibrium at the junction between curved (B) and faceted (C) section of the GB can be written in a form that takes into account Herring's torque terms [58]:

$$\gamma_C - \gamma_B \cdot \cos(\Delta\beta) + \frac{\partial\gamma_B}{\partial\beta} \cdot \sin(\Delta\beta) = 0, \quad (6)$$

where γ_B and γ_C are the energies of the B and C sections of the GB, respectively, and $\Delta\beta \approx 10^\circ$ is the in-plane inclination discontinuity at the junction. Substituting $\gamma_B \approx 0.94$ and $\gamma_C \approx 0.47$ (see Table 1) in Eq. (6) yields

$(\partial\gamma_B/\partial\beta) \approx 2.61$. It can be concluded that for GBs exhibiting high inclinational anisotropy, like GB no. 6, the value of Herring torques is comparable to the absolute value of the GB energy. It should be noted that Herring's torque terms considered here act in the plane of the sample surface and are caused by anisotropy of the GB energy. On the contrary, torques caused by the surface energy anisotropy should appear in Eq. (1). The surface anisotropy should cause strong surface faceting in the GB groove region, similar to the GB faceting considered here. Such faceted grooves were avoided in the present study (see selection criteria in Section 2.1), which provides a justification for the use of Eq. (1).

4.2.2. GB energy as a function of misorientational DOFs

It can be seen in Table 1 that several GBs with very different energies are close to the low- Σ misorientations ($\Sigma = 3$ $[111]$, 60° and $\Sigma = 9$ $[110]$, 38.9°). The GBs for which the parameters of the closest coincidence site lattice (CSL) GB are given in Table 1 fall, according to the Brandon criterion [27,59], within the stability region of respective CSL boundary. The fact that these near-CSL GBs exhibit very different energies underlines the importance of the GB plane inclination in determining the GB energy.

4.2.3. The role of GB plane

Representing the measured geometrical DOFs according to interface-plane scheme (see Table 1) has allowed us to find an interesting correlation: all but one high-energy GBs were of the $\{hk0\}||\{h'k'l'\}$ type. Qualitatively, this correlation can be related to the atomic pattern of $\{hk0\}$ planes which are built of alternating rows of Ni and Al atoms. If such a pattern is brought in contact with an arbitrary atomic plane $\{h'k'l'\}$, many unfavorable Ni–Ni or Al–Al bonds [60,61] at the GB may result, which would increase the GB energy.

4.2.4. The role of GB type (tilt or twist)

It is well known that a GB can be of a pure tilt, pure twist, or of a mixed type [10,18,19,24]. For pure tilt GBs the misorientation (tilt) axis is perpendicular to the GB plane normal: $[U, V, W] \perp \vec{n}_2$. Correspondingly, for pure twist GBs the misorientation (twist) axis is parallel to the GB plane normal: $[U, V, W] \parallel \vec{n}_2$. Let us define a new parameter, tilt/twist component (TTC), according to $TTC \equiv [U, V, W] \cdot \vec{n}_2$, where both vectors are normalized to unity. Its value varies from 0 for pure tilt GBs to 1 for pure twist GBs. The general case of $0 < TTC < 1$ describes a mixed GB, with TTC representing the fraction of the twist component in the GB. Using the data from Table 1, we have calculated TTC values for all 43 GBs investigated in this work. The dependence of the relative GB energy on TTC is shown in Fig. 9. This plot exhibits a wide scatter of the data, which is not surprising given that in this presentation four out of five

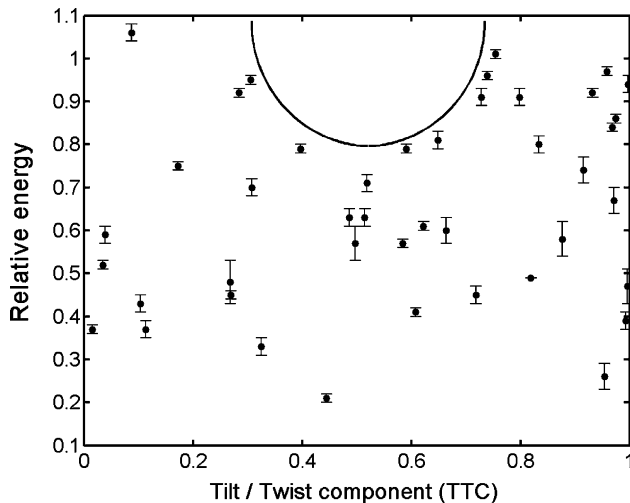


Fig. 9. Dependence of the relative GB energy on the tilt/twist component (TTC). TTC = 0 and TTC = 1 correspond pure tilt and pure twist GBs, respectively.

geometrical DOFs are convoluted into one parameter. A more informative method of visualizing the correlation between a GB property and GB geometrical DOFs has been proposed by Krakauer and Seidman [62]. They suggested to present the GB property as a function of the TTC (in the range from 0 to 1) and the disorientation angle (0 – 60°) in a three-dimensional plot, thus convoluting all five geometrical DOFs in two. Fig. 10 shows such dependence for γ_{rel} . The following trends can be recognized in Figs. 9 and 10:

- The GB energy reaches high values characteristic of random GBs at a disorientation of about 20° .
- Most of the high-energy GBs are concentrated in the twist region with $TTC > 1/2$.
- No high-energy GBs are observed in the vicinity of $TTC = 1/2$ for all disorientation angles.

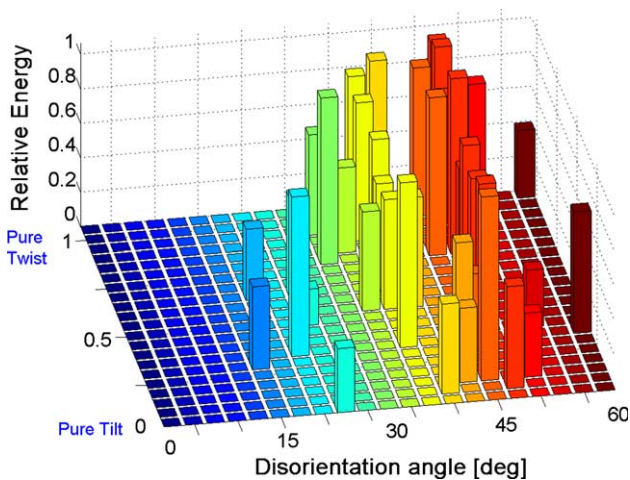


Fig. 10. Dependence of the relative GB energy on the tilt/twist component (TTC) and disorientation angle.

The first finding is consistent with the extended Read–Shockley model for high-angle GBs [58,63,64]. Both the first and second observations are in a good agreement with the results of Krakauer and Seidman [62]. They determined the Gibbsian interfacial excess of Si at 14 GBs in a single-phase Fe–3at.%Si alloy. Their results indicate that the transition from low-angle to high-angle GBs occurs at a disorientation of about 20° , and that twist GBs exhibit a higher level of segregation than their tilt counterparts. Those results are in a good agreement with the results of the present study, provided that a correlation exists between GB energy and GB segregation. Indeed, it is known that more impurities segregate to GBs of high energy, presumably because such GBs offer more segregation sites with a large free volume for oversized impurity atoms [65].

Regarding the third observation, it cannot be excluded that this is an artifact caused by poor statistics (relatively small number of GBs). On the other hand, at least for low-angle GBs, it can be argued that the superposition of a wall of edge dislocations and a grid of screw dislocations in a mixed GB with $TTC \approx 1/2$ gives rise to a variety of relaxation mechanisms of the complex dislocation network, which can lead to a decrease in the GB energy.

4.2.5. The existence of plane-matching GBs

As mentioned in Section 3.4, we found no evident correlation between plane matching and the GB energy. This is in contradiction to the commonly accepted view that plane-matching GBs have low energy. This contradiction confirms the importance of the inclinational DOFs of GBs, since the plane matching is only determined by three misorientational DOFs. The following plane-matching GBs have been found in our study: $\{211\}\{110\}$, $\{110\}\{110\}$, $\{211\}\{211\}$ and $\{211\}\{100\}$. The first three types of GBs exhibited both high and low energies, while all $\{211\}\{100\}$ GBs have high energies.

5. Conclusions

In this work, we have applied the thermal grooving technique in combination with EBSD and serial sectioning analyses to examine correlations between the energy of GBs in the Ni-rich NiAl intermetallic compound and their macroscopic geometrical DOFs. The experimental results have been compared with atomistic computer calculations of the GB and surface energies calculated using an EAM interatomic potential. The following conclusions can be drawn from this study:

1. The experimentally determined relative energies of large angle GBs range from 0.2 to 1.1. In this respect NiAl is different from elemental metals, in which the

relative GB energy usually does not exceed 0.5. The experimentally determined range of GB energies is in a good agreement with the results of atomistic simulations.

2. Twist GBs exhibit higher energies than their tilt counterparts, which is in agreement with the results of the segregation study by Krakauer and Seidman [62].
3. The energy of a selected large angle non-CSL GB has been found to vary over a wide range of 0.47–1.01, depending on its inclination. This finding underlines the important role of the inclinational DOFs in determining the GB energy, even for non-CSL (random) GBs.
4. The GB energy reaches high values characteristic of random large angle GBs for disorientations larger than 20°, which correlates well with the Read–Shockley dislocation model of low angle GBs.
5. General GBs with approximately equal tilt and twist components do not exhibit high energies.
6. The plane-matching GBs can have both low and high energy.

Acknowledgments

This work was supported by the Binational US–Israel Science Foundation under the Grant No. 2000066. Y.M. also wishes to acknowledge the support of the US Department of Energy through Grant No. DE-FG02-01ER45871. Dr. A. Fraczkiwicz from Ecole des Mines de Saint Etienne is heartily acknowledged for supplying us with the NiAl samples.

References

- [1] Miracle DB. *Acta Metall Mater* 1993;41:649.
- [2] Darolia R. *Intermetallics* 2000;8:1321.
- [3] Liu CT. *Mater Chem Phys* 1995;42:77.
- [4] *Metals handbook*. 10th ed., vol. 2; 1990. p. 913.
- [5] Hahn KH, Vedula K. *Scr Metall* 1989;23:7.
- [6] George EP, Liu CT. *J Mater Res* 1990;5:754.
- [7] Miller MK, Jayaram R, Camus PP. *Scr Metall Mater* 1992;26:679.
- [8] Cahn RW. *Intermetallics* 1998;6:563.
- [9] Rabkin E, Klinger L, Izyumova T, Berner A, Semenov V. *Acta Mater* 2001;49:1429.
- [10] Randle V. *Acta Mater* 1997;46:1459.
- [11] Randle V. *The role of the coincidence site lattice in grain boundary engineering*. London: The Institute of Materials; 1996.
- [12] Watanabe T, Tsurekawa S. *Acta Mater* 1999;47:4171.
- [13] Reitz WE. *JOM* 1998(Feb):39.
- [14] Palumbo G, Lehockey EM, Lin P. *JOM* 1998(Feb):40.
- [15] Schwartz AJ, King WE. *JOM* 1998(Feb):50.
- [16] Randle V. *JOM* 1998(Feb):56.
- [17] Randle V. *Acta Mater* 2004;52:4067.
- [18] Randle V. *The measurement of grain boundary geometry*. Bristol: Institute of Physics; 1993.
- [19] Wolf D, Lutsko JF. *Z Kristall* 1989;189:239.
- [20] Randle V, Ralph B. *J Mater Sci* 1986;21:3823.
- [21] Pumphrey PH, Bowkett KM. *Scr Metall* 1971;5:365.
- [22] Pumphrey PH, Bowkett KM. *Scr Metall* 1972;6:31.
- [23] Bollmann W. *Crystal lattices, interfaces, matrices*. Geneva: W. Bollmann; 1982.
- [24] Merkle KL, Wolf D. *MRS Bull* 1990(Sep):42.
- [25] Goodhew PJ. The relationship between grain boundary structure and energy. In: Balluffi RW, editor. *Grain boundary structure and kinetics*. Materials Park (OH): American Society for Metals; 1980.
- [26] Brandon DG, Ralph B, Ranganathan S, Wald MS. *Acta Metall* 1964;12:813.
- [27] Lojkowski W, Fecht HJ. *Prog Mater Sci* 2000;45.
- [28] Gleiter H. *Z Metall* 1970;61:282.
- [29] Priester L. *Rev Phys Appl* 1989;24:419.
- [30] Herrmann G, Gleiter H, Bäro G. *Acta Metall* 1976;24:353.
- [31] Sutton AP, Balluffi RW. *Acta Metall* 1987;35:2177.
- [32] Wynblatt P, Takashima M. *Interface Sci* 2001;9:265.
- [33] Saylor DM, El Dasher B, Sano T, Rohrer GS. *J Am Ceram Soc* 2004;87:670.
- [34] Klinger L, Rabkin E. *Interface Sci* 2001;9:55.
- [35] Levi G, Kaplan WD. *Acta Mater* 2002;50:75.
- [36] Amouyal Y. M.Sc. Thesis. Technion–Israel Institute of Technology; 2003.
- [37] Saiz E, Cannon RM, Tomsia AP. *Acta Mater* 1999;47:4209.
- [38] Schöllhammer JS, Chang L, Rabkin E, Baretzky B, Gust W, Mittemeijer EJ. *Z Metall* 1999;90:687.
- [39] Saylor DM, Rohrer GS. *J Am Ceram Soc* 1999;82:1529.
- [40] Randle V. *Scr Metall* 2001;44:2789.
- [41] Randle V. *Mater Charact* 1995;34:29.
- [42] Harris KE, Ebrahimi F, Garmestani H. *Mater Sci Eng A* 1998;247:187.
- [43] Watanabe T. *Philos Mag A* 1983;47:141.
- [44] Yamaura S, Igarashi Y, Tsurekawa S, Watanabe T. *Acta Mater* 1999;47:1163.
- [45] Martin JW, Doherty RD, Cantor B. *Stability of microstructure in metallic systems*. Cambridge: Cambridge University Press; 1997. p. 226.
- [46] Miracle DB, Darolia R. In: Westbrook JH, Fleischer RL, editors. *Intermetallics compounds: practice*, vol. 2. New York (NY): Wiley; 1994. p. 54.
- [47] Schöllhammer J, Baretzky B, Gust W, Mittemeijer E, Straumal B. *Interface Sci* 2001;9:43.
- [48] Skidmore T, Buchheit RG, Juhas MC. *Scr Mater* 2004;50:873.
- [49] Ference TG, Balluffi RW. *Scr Metall* 1988;22:1929.
- [50] Straumal BB, Polyakov SA, Bischoff E, Gust W, Baretzky B. *Acta Mater* 2005;53:247.
- [51] Mishin Y, Mehl MJ, Papaconstantopoulos DA. *Phys Rev B* 2002;65:224114.
- [52] Brown JA, Mishin Y. *Phys Rev B* 2003;67:195414.
- [53] Brown JA, Mishin Y. *Phys Rev B* 2004;69:195407.
- [54] Lozovoi AY, Mishin Y. *Phys Rev B* 2003;68:184113.
- [55] Mishin Y, Lozovoi AY, Alavi A. *Phys Rev B* 2003;67:014201.
- [56] Mishin Y, Farkas D. *Philos Mag A* 1998;78:29.
- [57] Xie X, Mishin Y. *Acta Mater* 2002;50:4303.
- [58] McLean D. *Grain boundaries in metals*. London: Oxford University Press; 1957.
- [59] Brandon DG. *Acta Metall* 1966;14:1479.
- [60] Petton G, Farkas D. *Scr Metall Mater* 1991;25:55.
- [61] Yan M, Vitek V, Chen SP. *Acta Mater* 1996;44:4351.
- [62] Krakauer BW, Seidman DN. *Acta Mater* 1998;46:6145.
- [63] Read WT, Shockley W. *Phys Rev* 1950;78:275.
- [64] Wolf D. *Scr Metall* 1989;23:1713.
- [65] Sutton AP, Balluffi RW. *Interfaces in crystalline materials*. Oxford: Clarendon Press; 1995.